

Phase estimation from transmitted-light DIC images using rotational diversity

Chrysanthe Preza†, Donald L. Snyder†, Frederick U. Rosenberger†
Joanne Markham, José-Angel Conchello

Institute for Biomedical Computing and †Department of Electrical Engineering
Washington University, St. Louis, Missouri

ABSTRACT

Differential-Interference-Contrast (DIC) microscopy is a powerful technique for the visualization of unstained transparent specimens, thereby allowing *in vivo* observations. Quantitative interpretation of DIC images is difficult because the measured intensity is nonlinearly related to the gradient of a specimen's optical-path-length distribution along the shear direction. The recent development of reconstruction methods for DIC microscopy permits the calculation of a specimen's optical-path-length distribution or phase function and provides a new measurement technique for biological applications.

In this paper we present a summary of our work on quantitative imaging with a DIC microscope. The focus of our efforts has been in two areas: 1, model development and testing for 3D DIC imaging; and 2, development of a phase-estimation method based on this model. Our method estimates a specimen's phase function using rotational-diversity DIC images, i.e. multiple DIC images obtained by rotating the specimen. Test objects were viewed with a conventional DIC microscope using monochromatic light, and images were recorded using a cooled CCD camera. Comparison of the images to model predictions show good qualitative and quantitative agreement. Results obtained from testing the phase-estimation method with 2D simulations and with measured DIC images demonstrate that an estimate of an object's phase function can be obtained even from a single DIC image and that the estimated phase becomes quantitatively better as the number of rotational-diversity DIC images increases.

Keywords: Computational Nomarski DIC microscopy, imaging theory, phase estimation, image reconstruction, 3D microscopy

1. INTRODUCTION

Transmitted-light Nomarski Differential-Interference-Contrast (DIC) microscopy^{1,2} is a widely used microscopy modality that was developed over forty years ago for the study of unstained transparent biological specimens not visible with ordinary transmitted-light microscopy. Attractive features of DIC microscopy are: 1, it does not require staining which can be toxic to some living specimens, and thus, prohibitive for *in vivo* applications; 2, it is particularly advantageous for four-dimensional imaging (three spatial dimensions and time) because sufficient light can be acquired in short exposures; and 3, it is available in many laboratories as it operates with a relatively inexpensive attachment on a conventional light microscope.

Over the last decades great effort has been devoted to the development of microscope systems and model-based computational methods that can provide quantitative measurements from images obtained with high quality, instrumentation-grade CCD cameras.³ Although the focus has been on the development of such methods for fluorescence microscopy (see for example Holmes,⁴ Chapters 13 and 24 in Pawley³ and references therein), some methods have been developed for bright-field microscopy,^{5,6} and a few for phase microscopy.⁷⁻⁹ Contrary to these microscopy modalities, DIC microscopy has been limited to qualitative and morphological applications until recently.

Further author information -

C.P.: Email: preza@wuibc.wustl.edu; WWW: <http://www.ibc.wustl.edu/~preza>; Telephone: 314-362-2135; FAX: 314-362-0234

The reason for this has been the lack of imaging models for DIC which, unlike other modalities, converts phase differences along a preferred system direction to intensity measurements. The intensity distribution in measured DIC images is given by a nonlinear function of approximately the spatial gradient of a specimen’s optical-path-length distribution (integral of refractive index over length) along the direction of shear (perpendicular to the optical axis). Clearly, DIC imaging is direction sensitive and does not provide quantitative information about a specimen’s optical-path-length distribution. Furthermore, the resolution in DIC images is degraded by the blurring effects of the microscope’s objective lens, as in any microscopical modality.

In the last decade there have been only a few attempts to develop reconstruction methods for DIC microscopy^{10–12} due to the complexity of the nonlinear DIC reconstruction problem. Unfortunately, the success of these methods has been limited because they are based on simplified imaging models. More specifically, two of the methods^{11,12} are based on a linear approximation of the model that may be appropriate only for some applications in which weak-phase flat specimens are studied.¹² Also, because these methods use a single DIC image for the reconstruction, they are sensitive to the orientation of the object with respect to the DIC shear direction.

Recently, we reported a phase-estimation method for DIC microscopy which overcomes the direction sensitivity of DIC imaging.¹³ The method estimates a specimen’s optical-path-length distribution using rotational diversity: i.e. multiple DIC images obtained at different rotations of the specimen. The method is based on a general imaging model for three-dimensional (3D) DIC imaging which we derived from basic principles and was presented in a previous publication.¹⁴ Our objective is to obtain a quantitative estimate of the spatial optical-path-length variations of the specimen, which is more fundamental than the gradient of the optical-path-length that is produced directly with the microscope and which microscope users normally view. To this end we have been testing our model and method with simple physical phantoms (calibration objects).

In this paper, we report results from testing our model and phase-estimation method by comparing real DIC images obtained from physical phantoms to model predictions and by comparing estimated phase images to phantoms. The paper is organized as follows. Section 2 summarizes our phase-estimation method and the imaging model on which the method is based. Section 3 describes the data acquisition and simulation studies performed to test the model and our method’s ability to estimate phase functions from DIC images of simple phantoms. Finally, Section 4 summarizes results obtained from these studies.

2. BACKGROUND

2.1. DIC microscope operation

In a DIC microscope, key optical components (a polarizer, an analyzer and two Wollaston prisms) create the necessary conditions so that a two-dimensional (2D) image is formed from the interference of two mutually coherent waves that have a lateral differential displacement of a few tenths of a micrometer, called the *shear*, and are phase-shifted relative to each other. The phase difference between the two waves is due to variations in the refractive index across the specimen. These phase variations are converted to intensity variations in the DIC image and, thus, the intensity in the DIC image is approximately the square of the derivative of the specimen’s optical-path-length distribution along the direction of shear (perpendicular to the optical axis). Clearly, DIC imaging is sensitive to the orientation of specimen features with respect to the direction of shear. Furthermore, the contrast in the DIC image may be controlled by adjusting a system parameter called the *bias retardation* which is a uniform phase shift between the two waves (for a detailed description of the DIC microscope operation see the listed publications^{2,1,15} and references therein). This property of DIC imaging creates a shadow-cast effect in DIC images which gives a false 3D impression and makes quantitative interpretation of DIC images difficult.

2.2. Model for image formation

The success of a model-based reconstruction method in inverting the imaging formation process critically depends on the adequacy of the imaging formation model on which the method is based. Our interest in developing a reconstruction method for transmitted-light DIC microscopy, based on rotational diversity, led us to the development of an imaging model (described in detail in previous publications^{14,13}) which we summarize here for completeness.

Without loss of generality, we model specimen rotation as a rotation of the point-spread function (PSF),

$$h(x, y, z) = \frac{1}{2} \left[e^{-j\Delta\theta} p(x - \Delta x, y, z) - e^{j\Delta\theta} p(x + \Delta x, y, z) \right], \quad (1)$$

by an angle, γ_k , defined as the angle that the shear direction makes with the horizontal axis, where $2\Delta\theta$ is the bias retardation (in radians), $2\Delta\mathbf{x}$ is the shear, and $p(\mathbf{x})$ is the coherent PSF of the microscope's objective lens (see Goodman,¹⁶ p. 111). This is equivalent to modeling rotation of the direction of shear for a fixed specimen.

Using a finite-dimensional discrete representation for the k^{th} -diversity DIC-image intensity, $i_k(\mathbf{x})$, of a specimen characterized by a transmission function $f(\mathbf{x}) = e^{-j\phi(\mathbf{x}_o)}$ and illuminated by a quasi-monochromatic source with a mean wavelength λ and intensity $a(\boldsymbol{\xi})$ (defined to have a zero value outside the circular aperture of the condenser lens), we write

$$i_k(\mathbf{x}) = \sum_{\boldsymbol{\xi} \in \Xi} \alpha(\boldsymbol{\xi}) \left| \sum_{\mathbf{x}_o \in \chi} f(\mathbf{x}_o) h_k(\mathbf{x} - \mathbf{x}_o) h_c(\boldsymbol{\xi}; \mathbf{x}_o) \right|^2, \quad (2)$$

where f is the object array with samples of $e^{-j\phi(\mathbf{x}_o)}$, h_k is the array with samples of the k^{th} rotation of the PSF, α and h_c are arrays that specify the illumination, \mathbf{x} and \mathbf{x}_o are 3D coordinates that take values on the set $\chi = \{0, 1, \dots, N-1\}^3$, where N is the number of elements in each dimension of the object and image space, and $\boldsymbol{\xi}$ takes values on $\Xi = \{0, 1, \dots, M-1\}^2$, where M is the number of elements in each dimension of the condenser aperture plane. Thus, K rotational-diversity images, $i_k(\mathbf{x})$ for $k = 0, \dots, K-1$, have a different shear direction defined by the rotation angle γ_k . In practice, the direction of shear is fixed and rotational-diversity DIC images are obtained by rotating a specimen. Therefore, measured images need to be rotated computationally prior to processing in order to account for this difference between the model and the measured data.

Equation 2 is a general formulation of the intensity in the image plane of a DIC microscope that describes partially coherent imaging. The limiting cases of the model for coherent and incoherent illumination can be obtained by specifying the intensity, $\alpha(\boldsymbol{\xi})$, of the source. The coherent-illumination limit is obtained by letting $\alpha(\boldsymbol{\xi}) = \delta(\boldsymbol{\xi})$, a 2D Dirac delta function. This limit gives

$$i_k(\mathbf{x}) = \left| \sum_{\mathbf{x}_o \in \chi} f(\mathbf{x}_o) h_k(\mathbf{x} - \mathbf{x}_o) \right|^2, \quad (3)$$

which we refer to as the point-aperture model, because it corresponds to closing the condenser aperture down to a single point. Our initial tests have been focused on the point-aperture model because it is easier to compute than the general model for partially-coherent imaging. Results from previous tests showed a qualitative agreement between model predictions obtained with this model and measured images, reported in an earlier publication.¹⁴

2.3. Phase-estimation method

We have derived an iterative phase-estimation method to invert the DIC image formation process using rotationally-diverse images. Details on the method were presented in an earlier publication,¹³ but for completeness, the method is summarized here.

An estimate of the object's phase function, $\phi(\mathbf{x}_o)$, is obtained by minimizing the cumulative, uniformly weighted, squared-error,

$$E = \sum_{k=0}^{K-1} \sum_{\mathbf{x} \in \chi} [d_k(\mathbf{x}) - i_k(\mathbf{x})]^2, \quad (4)$$

between K measured rotational-diversity images, $d_k(\mathbf{x})$, and the theoretical images, $i_k(\mathbf{x})$, predicted by the model in Equation 2. For this we use the well-known conjugate gradient method (see Aoki,¹⁷ p. 118) which starts from some initial guess ϕ^0 and, at iteration m , produces a new estimate for ϕ by minimizing the cost function, E , along the direction \mathbf{h}^m :

$$\phi^{m+1} = \phi^m - \beta_m \mathbf{h}^m \quad m = 0, 1, \dots \quad (5)$$

where β_m is the step size. The computation of of the direction \mathbf{h}^m and of the step size, β_m , requires evaluation of the gradient vector, $\nabla E(\phi^m)$, and the Hessian matrix of E , respectively. Because it is not computationally practical to evaluate the Hessian matrix, an estimate for β_m is evaluated numerically instead using a modified line-search method based on a polynomial approximation method (Aoki,¹⁷ p. 148). For a given \mathbf{h}^m , three points of the cost function are evaluated so that they define an interval in which the cost function has a minimum. Because the minimum of a quadratic function fitted through the three points closely approximates the minimum of the cost function, the step size that minimizes this quadratic function can be used.

In general, only relative phase (or phase difference) can be estimated and thus, the initial guess, ϕ^0 , used in Equation 5 affects the estimated absolute phase value. Phase estimated with our present algorithm from synthetic images of 2D test structures converges to a very good approximation of the specimen (up to an unknown additive constant) in the order of a few hundred iterations, at which point the change per iteration is extremely small. We have found that more iterations as well as a larger set of rotational-diversity images are required to resolve closely spaced points.¹³ Although the method was derived for 3D-phase estimation, our simulations so far have been 2D because effective 2D-phase estimation is useful in some applications and, also, it is a prerequisite to 3D-phase estimation.

3. METHODS

DIC images from two simple phantom specimens were acquired in order to test the point-aperture model and the phase-estimation method. First, a 2D phantom with a shallow groove was used for quantitative tests of both the model and the phase-estimation method. Second, a 3D phantom specimen that consists of two crossed bars was used to test the rotational-diversity model by comparing multiple DIC images acquired at different specimen rotations to model predictions.

3.1. Phantom specimens

The phantom specimens were constructed at the laboratory of Dr. Robert Krchnavek (Electrical Engineering department, Washington University, St. Louis, MO). The simple 2D groove phantom was fabricated by etching 2 parallel grooves in a glass slide, each groove approximately $7 \mu\text{m}$ ($\pm 60 \text{ nm}$) wide and 60 nm ($\pm 5 \text{ nm}$) deep. Based on the etching process, the grooves are expected to have sharp edges. The grooves were measured with a stylus profilometer (Alpha Step, Tencor Instruments) to be approximately 55-65 nm deep.

The 3D cross phantom was constructed from resins with well known refractive indices, and it consists of two bars with width, height, and thickness approximately $6 \mu\text{m}$, and refractive index slightly higher than the refractive index of the medium that surrounds them (Figure 1).

3.2. Data acquisition

A DIC image of the groove phantom was acquired by Erik van Munster (Academic Medical Center of the University of Amsterdam, the Netherlands) using an Ortholux II (Leitz, Germany) DIC microscope with a Leitz DIC 25x/0.5-NA dry objective lens and a dry condenser lens with the condenser aperture open. The DIC bias was set to be approximately $\pi/2$ radians by rotating a polarizer (de Senarmont method¹⁸). A band-pass filter (MAD8-1, Schott Glaswerke, Germany) with peak at 550 nm and bandwidth 8 nm around the peak was fitted in front of the light source for monochromatic illumination. The images were acquired with a cooled CCD camera (Lambert Instruments, the Netherlands) equipped with a Kodak KAF0400 CCD chip ($9\text{-}\mu\text{m}$ well size). The effective pixel size in the recorded images is $0.36 \mu\text{m}$. A DIC image of small latex beads (460 nm in diameter) was also measured at bias setting equal to $\pi/2$ radians for the determination of the shear parameter. Calibration images, I_{min} and I_{max} , were also acquired at bias of 0 and π radians respectively of an empty region on the slide using the same exposure time as for the other images. These images were used to correct the measured DIC images for CCD camera dark current and non-uniform flat-field response, and to normalize the DIC image values. For the correction, I_{min} is subtracted from each DIC image, then the result is divided by $(I_{max} - I_{min})$.

The rotational-diversity DIC images of the cross phantom were acquired using an Olympus IMT2 inverted microscope (Olympus Corporation, N.Y.) with the IMT2-NIC attachment for DIC, a 10x/0.3-NA dry objective lens, a 0.55-NA dry condenser lens with a closed aperture, and a cooled CCD camera (Photometrics Ltd., Tucson, Ariz.) equipped with a Kodak KAF1400 CCD chip ($6.8\text{-}\mu\text{m}$ well size). A band-pass filter with peak at 535 nm and FWHM equal to 64.5 nm (IF550, Olympus) was placed in front of the light source for monochromatic illumination. The bias setting, controlled by sliding the Wollaston prism, is not calibrated on this microscope and, thus, the required correction images at 0 and π radians were not acquired. The effective pixel size in each 2D recorded image is $0.68 \mu\text{m}$. The cross was imaged at four different orientations. First, the two bars of the cross were aligned with the vertical and horizontal axis (Figure 1, right panel). The cross was then rotated manually (by rotating the specimen slide) by approximately 13, 32 and 47 degrees clockwise. A through-focus series of 2D images was acquired at steps of $3 \mu\text{m}$ for each orientation of the cross.

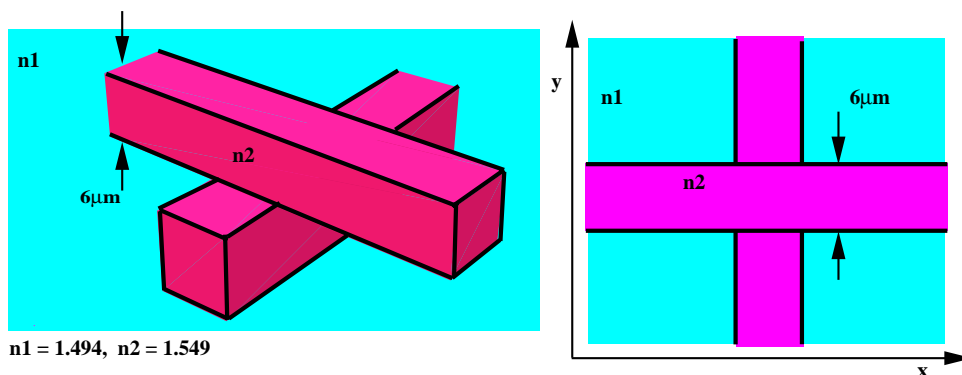


Figure 1. Schematic of the 3D phantom specimen with crossed bars.

3.3. Model predictions and phase estimation

Model predictions were obtained via simulations using the point-aperture model (Equation 3), because it is easier to compute than the general model, and computer-generated phantoms based on the physical description of our phantom specimens. The theoretical PSFs (Equation 1) were evaluated at different shear angles with shear distance equal to approximately $1 \mu\text{m}$, light wavelength equal to 550 nm and various bias values. The shear for the $25\times/0.5\text{NA}$ lens was empirically determined from the DIC image of a small latex bead (460 nm in diameter) to be equal to $1.017 \mu\text{m}$ along the 45 -degree axis (Figure 2) using a method similar to the one described by van Munster *et al.*¹²

Two synthetic DIC images of the 2D groove phantom were generated: one with the shear in the same direction as in the measured image, and the other with the shear direction rotated by 90 degrees. The bias, $2\Delta\theta$, was estimated from the average value, I_b , of a region in the corrected DIC image with no specimen using the expression $\Delta\theta = \sin^{-1}(\sqrt{I_b})$; it is easy to show that Equation 3 reduces to $i_k(x) = \sin^2(\Delta\theta) = I_b$ for $f(x_o) = 1$. The estimated bias value of 1.252 radians was used instead of the set value of $\pi/2$ radians. Phase images were estimated from both the measured and synthetic DIC images of the groove phantom using a uniform initial guess (an image with a constant value).

For the cross phantom, four 3D images were computed with a rotating shear direction that corresponds to the specimen rotation mentioned above. The synthetic DIC images were then rotated in order to convert shear-direction rotation to specimen rotation, thereby allowing comparison with the measured images. An estimated bias of -0.001 radians was used.

Synthetic rotational-diversity DIC images of a 2D computer-generated phantom that corresponds to a projection of the two crossed-bars in the cross phantom in a single plane were also generated for bias setting equal to 0.3 radians. Different sets of these images with varying number of diversity images, K , were used to estimate the phase of the phantom with our method. Phase images were estimated with $K = 1$ using an image with the direction of shear along the horizontal axis, $K = 2$ using images at 90 -degree shear rotations, and $K = 4$ with 45 -degree shear rotations. In all cases a uniform initial guess was used.

The current, nonoptimized implementation of our method, based on the point-aperture model, requires approximately 1 hour of processor time on an SGI R10000 180 MHz processor for computation of one 64×64 -pixel 2D phase image from 4 rotational-diversity DIC images with 100 iterations. With the present implementation, computing time per iteration is proportional to the number of DIC images and to the square of the number of pixels in the image. Implementation modifications that allow processing an image in small parts can reduce the complexity to be proportional to a constant times the number of pixels in the image.

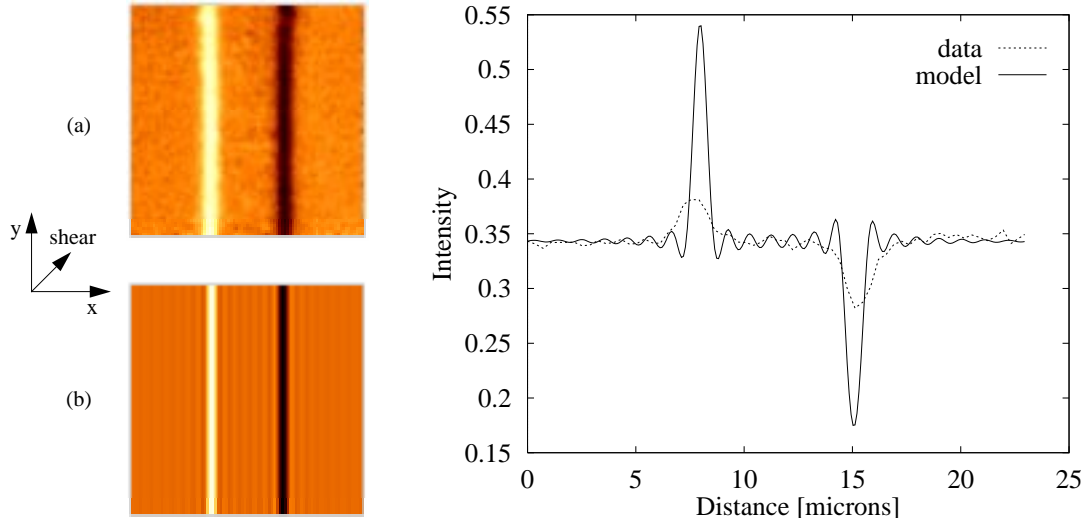


Figure 2. Comparison of DIC images of the groove phantom: (a) measured DIC image from the physical phantom using a 25x/0.5NA lens (shear=1.0 μm), 550 nm illumination wavelength, and an open condenser aperture; (b) synthetic DIC image generated from the point-aperture DIC image formation model (Equation 3 with shear angle $\gamma_k = \pi/4$ radians) and the geometric description of the phantom and the estimated imaging conditions. In both images, the direction of shear is at 45 degrees with respect to the horizontal axis. Horizontal profiles through the measured image (data) and the synthetic image (model) are compared in the right panel.

4. RESULTS

4.1. Model testing

Comparison of the measured DIC image and the model prediction of the groove phantom (Figure 2) shows good qualitative agreement. The two images appear to be similar and show a distance of approximately 7 μm between the groove edges. However, quantitative differences are evident from the profiles shown in Figure 2. The measured DIC image has a much lower and slightly wider peak than the synthetic DIC data. Furthermore, the model prediction shows oscillations that are characteristic of coherent imaging (Goodman,¹⁶ p. 131-132).

This mismatch could be attributed to several differences between the actual imaging conditions and the ones assumed in the generation of the synthetic image: 1, condenser aperture size - we have used the model case that assumes a point-aperture (i.e. coherent imaging) because it is easy to compute while the image was obtained with an open condenser aperture; 2, errors in the bias value and the shear value and direction; 3, PSF errors; and 4, deficiencies in the imaging model.

To test the rotational-diversity model, we compare measured images of the cross phantom with 3D model predictions. A quantitative comparison was not possible at this point due to the lack of a rotational stage and microscope calibration. For simplicity we show only 2D images (Figure 3). Each 2D image is a cut through the middle of a 3D volume. Several similarities between the images are noted with respect to object features that are present in the images. At the first orientation of the phantom the shear direction makes a 45-degree angle with both bars and, thus, the edges of both bars are visible (Figure 3a). As the phantom is rotated clockwise the phase-gradient information of one of the bars dominates making that bar more visible in the image. Finally, only the bar that is oriented perpendicular to the direction of shear is visible while the other one, along the direction of shear, disappears (Figure 3d). The asymmetry evident in the measured images (i.e. the difference in the bar edges in Figure 3d, top row) suggests that the bars do not have a square cross section which was assumed for the computer-generated phantom used in the model predictions.

4.2. Evaluation of the phase-estimation method

Results obtained from applying the phase-estimation method to measured and synthetic DIC images are presented in this section. Estimated phase images from DIC images of the groove phantom compare well to the actual phantom

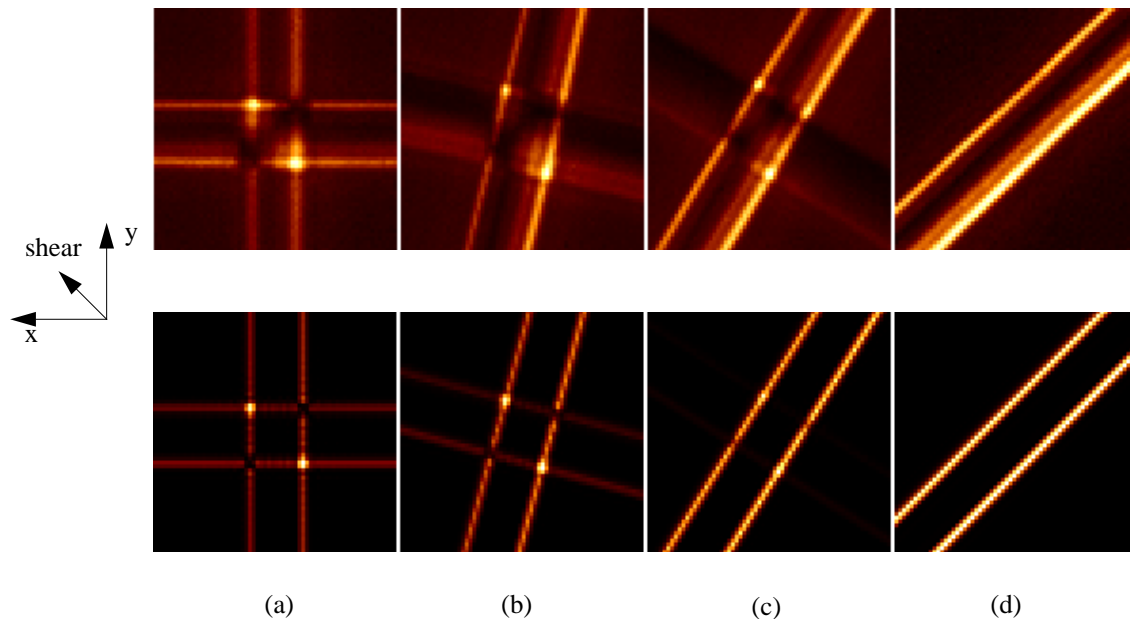


Figure 3. Measured DIC images (top row) of the 3D cross phantom specimen using a 10x/0.3NA lens, 550 nm illumination wavelength, and a closed condenser aperture; and model predictions (bottom row) of the DIC image of the phantom specimen shown in Figure 1 obtained with a 3D point-aperture model, with PSF bias equal to -0.001 radians at different orientations of the phantom: (a) the phantom is oriented as shown in the right panel of Figure 1; (b) the phantom is rotated by 13 degrees clockwise from position (a); (c) the phantom is rotated by 32 degrees from position (a); and (d) the phantom is rotated by 47 degrees from position (a). The direction of shear in all images is approximately perpendicular to the bar shown in (d).

(Figure 4). However, there are some differences evident in the profiles through the estimated phase images and the phantom cross-section. Some of these differences are expected because of the observed mismatch between the measured and synthetic DIC image (Figure 2). The estimated relative phase value, ϕ , is converted to thickness (or groove depth) from the expression $\phi = 2\pi\Delta n t/\lambda$, where the refractive index difference is $\Delta n = 0.522$, and the illumination wavelength is $\lambda = 550$ nm. A depth of 60 nm was assumed for the computer-generated phantom shown in Figure 4b. A groove depth of approximately 56.3 nm was computed from the phase image (Figure 4a) estimated from the measured DIC image; this estimated depth value falls within the depth range (55-65 nm) that was determined by the profilometer measurement. However, the phase estimate from the measured DIC image does not predict sharp edges for the groove. This may be expected because the peaks in the measured DIC image are wider than those in the synthetic image (Figure 2).

The estimated phase images from the synthetic DIC images approximate the phantom's phase very well; the oscillations are due to the sharp edges and they are consistent with the Gibbs' phenomenon. Because this simple phantom changes only in one direction, the phase-estimation method does not benefit from the additional information provided by rotational diversity. The estimated phase image from two synthetic DIC images with shear angle separation of $\pi/2$ radians (Figure 4c) is only marginally better than the phase estimate from a single DIC image (Figure 4d). This is, of course, expected because one DIC image can capture all the gradient information for the groove except when the groove is oriented along the direction of shear.

To demonstrate the benefit of rotational-diversity in cases where the object has structures in more than one direction, we have estimated phase images from synthetic DIC images (Figure 5) of a 2D projection of the cross phantom shown in Figure 6a. Because in the DIC image shown in Figure 5a the direction of shear is parallel to one of the bars of the cross, little or no information about the horizontal bar is present in the image. Thus, as expected, the estimated phase image from this single DIC image (Figure 6d) does not show the cross-bar structure of the phantom, and it is less accurate than the phase images computed from two or more DIC images (Figure 6). From Figure 6, we note that the oscillations in the background of the phase image obtained using four DIC images (Figure 6b) appear to be larger than the oscillations in the phase image from two DIC images (Figure 6c). We believe

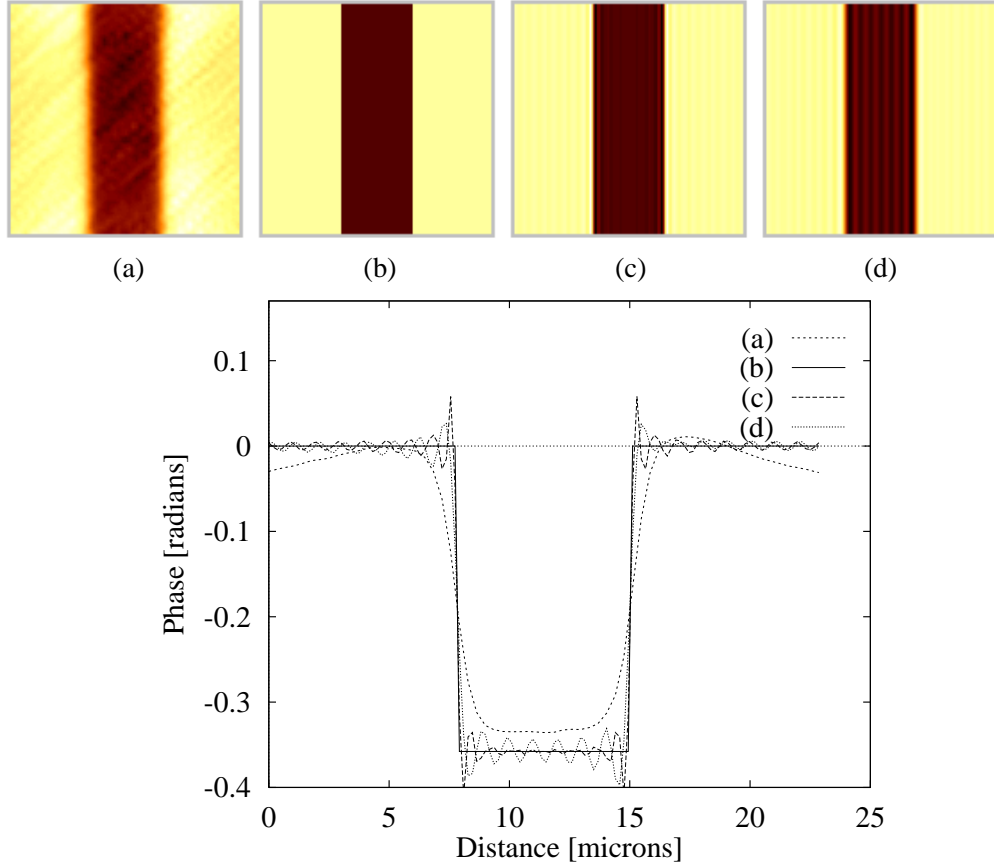


Figure 4. Comparison of estimated phase images of the groove phantom: (a) estimated phase from the measured DIC image of the groove phantom shown in Figure 2a; b) computer-generated phantom of the groove with width of $7 \mu\text{m}$ and depth 60 nm ; c) estimated phase from two synthetic DIC images at 90° shear angle separation which were generated from (b); and, d) phase estimated from a single synthetic DIC image shown in Figure 2b. Horizontal profiles through the images are compared in the bottom panel. Profile (a) is the row average of image (a). The relative phase due to the groove with respect to the background is 0.358 radians (computed from $\phi = 2\pi\Delta n t/\lambda$ with: refractive index difference, $\Delta n = 0.522$; illumination wavelength, $\lambda = 550 \text{ nm}$; and thickness, $t = 60 \text{ nm}$).

that this is because the oscillations in the DIC images with shear angle at 45° with respect to both bars (Figure 5b and d) are larger than the oscillations in the the images with shear angle at 0° and 90° (Figure 5a and c). These oscillations arise because the microscope passes a limited band of spatial-frequency components and are characteristic of coherent imaging (Goodman,¹⁶ p. 131-132). Because the phase-estimation method does not use any prior information on the phase function, it is unable to remove these oscillations. Also, the current implementation of our method does not include any regularization which could reduce the oscillations.

It is clear from Figure 6 that a significant improvement in the estimated phase image is achieved when two DIC images at 90° -degree shear angle separation are used. However, the benefit of using more than two rotational-diversity images is not evident in the phase images estimated from these noiseless synthetic images of the cross phantom which has $\pi/2$ radians rotational symmetry.

5. SUMMARY AND CONCLUSIONS

We have shown results from testing a simple case of our more general model with two physical phantom specimens: a 2D groove phantom and a 3D cross phantom. The 2D phantom was also used as a vehicle for assessment of quantitative phase estimation. Conclusions from these tests are summarized in four main areas:

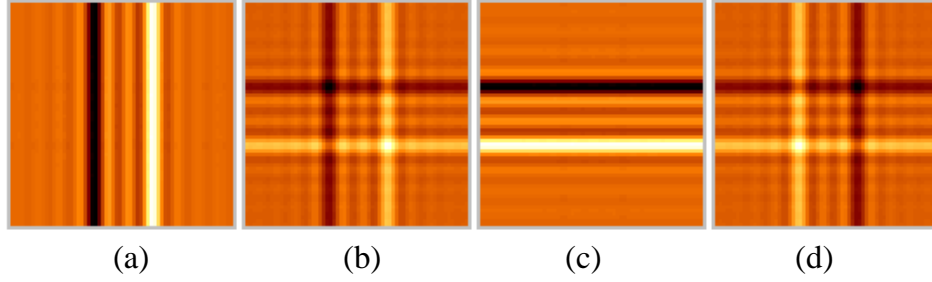


Figure 5. Synthetic rotational-diversity DIC images of a 2D projection of the cross phantom with different orientation of the shear. The shear is along the horizontal axis in (a), and it is rotated every 45 degrees clockwise from (a) to (d).

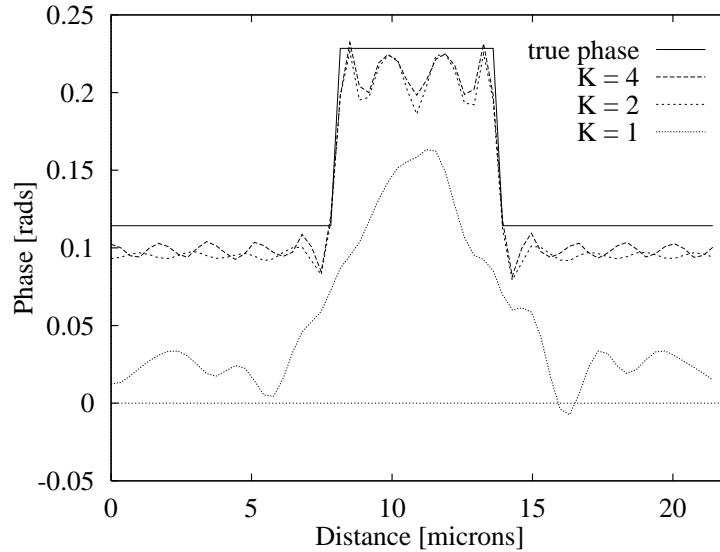
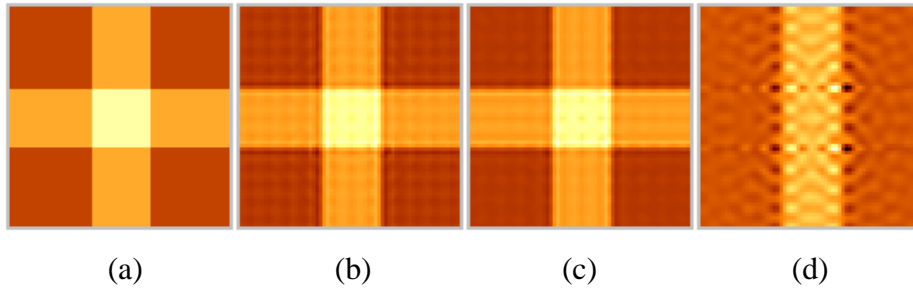


Figure 6. Phase image of a 2D computer-generated cross (a), and estimated phase images of the 2D cross obtained from the diversity images shown in Figure 5: (b) from four images ($K = 4$) with 45-degree shear rotation; (c) from two images ($K = 2$) with orthogonal shear direction; and (d) from a single image ($K = 1$) with the direction of shear along the horizontal axis shown in Figure 5a. Horizontal profiles taken through the center of the images are compared at the bottom panel. The baseline offset of the profiles through the estimated phase images for $K = 2$ and $K = 4$ is due to the initial guess.

1. A quantitative comparison between real DIC images acquired with the 2D groove phantom specimen and model predictions obtained with the coherent limit of our general imaging model (point-aperture model) has shown a number of similarities that suggest that while our model is not perfect, it does capture the major features. Two of the factors that may be responsible for the observed differences in our comparison are: 1, the point-aperture assumption used by the model case that we are testing initially; and 2, errors in the estimated imaging parameters (bias and shear). Our next step is to reduce the effect of these factors. First, a better estimate of the bias and shear parameters can be obtained by using information from multiple DIC images of the groove phantom obtained with different illumination wavelengths, and by changing the groove's refractive index (for example by putting water in the groove). A better estimate of the bias and shear should also lead to a more accurate estimate of the groove's phase. Second, by generating synthetic DIC images with our general open-aperture model, we expect that the match between model and data will improve.
2. Despite the observed differences in the model comparison, results from testing the ability of our method to estimate the phase function of the 2D groove phantom from a measured DIC image have been very encouraging and suggest that the phase-estimation method works; the width and depth of the groove in the estimated phase image are within 6% (which is within measurement error) of the actual values.
3. Comparison of measured rotational-diversity DIC images of a 3D cross phantom to 3D model predictions has confirmed that our imaging model can predict the DIC-imaging direction sensitivity.
4. Results obtained with the phase-estimation method from rotational-diversity synthetic DIC images of a 2D cross show significant improvements when two DIC images (with orthogonal shear angles) are used, rather than a single image. The benefit of using more than two DIC images for phase estimation is not evident for this simple phantom with rotational symmetries that we have used. We expect that additional rotational-diversity images will be beneficial for phase estimation from images of real specimens because they do not possess rotational symmetries and because of the effects of noise. We are currently investigating the benefits of rotational diversity in phase estimation from images of real specimens.

6. ACKNOWLEDGEMENTS

This research was supported in part by the National Institutes of Health under research grants RR 01380, BTA-SIO-RR 10412, RO1 GM49798, and by Washington University. The authors wish to thank Robert Krchnavek, Richard Livingston and Brian Faircloth for the construction of the phantom specimens and for the profilometer measurement of the groove phantom. Special thanks are extended to Erik van Munster for acquiring the DIC image of the groove phantom specimen and the calibration images, and for insightful discussions.

REFERENCES

1. R. D. Allen, G. B. David, and G. Nomarski. "The Zeiss-Nomarski Differential Interference Equipment for Transmitted-Light Microscopy". *Zeitschrift für Wissenschaftliche Mikroskopie und Mikroskopische Technik*, 69(4):193–221, 1969.
2. W. Lang. "Nomarski Differential Interference Contrast Microscopy". *A Collection of Four Articles from Zeiss Information, Carl Zeiss, 7082 Oberkochen, West Germany*, 1968.
3. J. B. Pawley, editor. *Handbook of Biological Confocal Microscopy*. Plenum Press, New York, 1995.
4. T. J. Holmes and Y.-H. Liu. "Image Restoration for 2-D and 3-D Fluorescence Microscopy". In A. Kriete, editor, *Visualization in Biomedical Microscopies*, pages 283–327. Weinheim, New York, 1992.
5. F. Macias-Garza, A. C. Bovik, K. R. Diller, S. J. Aggarwal, and J. K. Aggarwal. "Digital Reconstruction of Three-Dimensional Serially Sectioned Optical Images". *IEEE Transactions on Acoustics, Speech, and Signal Processing*, 36(7):1067 – 1075, July 1988.
6. B. Willis, B. Roysam, J. N. Turner, and T.J. Holmes. "Iterative, Constrained 3-D Image Reconstruction of Transmitted Light Bright-Field Micrographs based on Maximum Likelihood Estimation". *Journal of Microscopy*, 169, pt 3:347–361, 1993.
7. T. Noda, S. Kawata, and S. Minami. "Three-Dimensional Phase Contrast Imaging by an Annular Illumination Microscope". *Applied Optics*, 29(26):3810–3815, 1990.

8. I. Nemoto and A. Takahashi. "Methods of Improving the Images in Phase-Contrast Microscopy: Theory and Computer Simulation". *Journal of the Optical Society of America A*, 8(3):511–519, 1991.
9. T. Noda, S. Kawata, and S. Minami. "Three-Dimensional Phase-Contrast Imaging by a Computed-Tomography Microscope". *Applied Optics*, 31(5):670–674, 1992.
10. T. J. Holmes and W. J. Levy. "Signal-Processing Characteristics of Differential-Interference-Contrast Microscopy". *Applied Optics*, 26(18):3929–3939, 1987.
11. K. Dana. "Three Dimensional Reconstruction of the Tectorial Membrane: An Image Processing Method Using Nomarski Differential Interference Contrast Microscopy". Master's thesis, Massachusetts Institute of Technology, Massachusetts, 1992.
12. E. B. van Munster, L. J. van Vliet, and J. A. Aten. Quantitative Interferometric Imaging Using a Conventional Differential Interference Contrast Microscope. In A. V. Priezhev, T. Asakura, and R. C. Leif, editors, *Optical Diagnostics of Biological Fluids and Advanced Techniques in Analytical Cytology*, volume Proc. SPIE 2982, pages 458–467, 1997.
13. C. Preza, D. L. Snyder, and J.-A. Conchello. Image Reconstruction for Three-Dimensional Transmitted-Light DIC Microscopy. In C. J. Cogswell, J.-A. Conchello, and T. Wilson, editors, *Three-Dimensional Microscopy: Image Acquisition and Processing IV*, volume Proc. SPIE 2984, pages 220–231, 1997.
14. C. Preza, D. L. Snyder, and J.-A. Conchello. Imaging Models for Three-Dimensional Transmitted-Light DIC Microscopy. In C. J. Cogswell, G. S. Kino, and T. Wilson, editors, *Proceedings of the IS&T/SPIE symposium on Electronic Imaging, Science and Technology*, volume 2655, pages 245–257, 1996.
15. M. Pluta. *Advanced Light Microscopy: Specialized Methods*, pages 146–197. Elsevier, Amsterdam, 1989.
16. J. W. Goodman. *Introduction to Fourier Optics*. McGraw-Hill Book Company, New York, 1968.
17. M. Aoki. *Introduction to Optimization Techniques*. The Macmillan Company, New York, 1971.
18. C. J. Cogswell, N. I. Smith, K. G. Larkin, and P. Hariharan. Quantitative DIC Microscopy Using a Geometric Phase Shifter. In C. J. Cogswell, J.-A. Conchello, and T. Wilson, editors, *Three-Dimensional Microscopy: Image Acquisition and Processing IV*, volume Proc. SPIE 2984, pages 72–81, 1997.